

Special Issue of the 8th International Advances in Applied Physics and Materials Science Congress (APMAS 2018)

Investigation of Light Trapping from Porous Silicon Surface for the Enhancement of Silicon Solar Cell Performance

A.F.A. RAHIM^{a,*}, M.A. AHMED^a, N.S.M. RAZALI^a, R. RADZALI^a, A. MAHMOOD^b,
I.H. HAMZAH^a AND E. NOORSAL^a

^aFaculty of Electrical Engineering, Universiti Teknologi MARA Cawangan Pulau Pinang,
13500, Permatang Pauh, Penang, Malaysia

^bDepartment of Applied Sciences, Universiti Teknologi MARA Cawangan Pulau Pinang,
13500, Permatang Pauh, Penang, Malaysia

In this work, an innovative porous silicon structure was utilized as an effective antireflective layer for silicon solar cell construction. Silvaco technology computer aided design tools were used to construct the three structures of the porous silicon layers which were no porous, single porous, and double porous. Athena process simulator was used to create the non-porous silicon structure (as control device) and the single porous silicon structure, while the double porous structures were created at the *n*-type and *p*-type surfaces of the silicon solar cell by using the device editor (Devedit) tools. The three simulated structures were imported to the Atlas device simulator tools to simulate the current–voltage (*I*–*V*) characteristic and the spectral response of the solar cell. The simulation results of the three structures were compared with the fabrication results obtained by Ramizy et al. Finally, the efficiency extracted from the double porous solar cell is 9.55%, the single porous is 9.32%, and the no porous structure exhibited 4.83% efficiency. The double porous silicon solar cell showed an ability to effectively trapping the light collected in the solar cell and thereby improve the efficiency of the solar cell compared to the no porous and the single porous silicon structure.

DOI: [10.12693/APhysPolA.135.637](https://doi.org/10.12693/APhysPolA.135.637)

PACS/topics: Silvaco TCAD, Athena, Devedit, porous silicon, surface texturing

1. Introduction

A solar (or photovoltaic) cell is used to produce the electricity by converting the sun energy to electrical energy. There are three generations of the solar cells, the first generation uses wafer based crystalline silicon (c-Si) and monocrystalline silicon. The second generation of the solar cell uses the thin film technology. The third generation uses high-efficiency thin film technology (advanced thin films). To improve the efficiency of the solar cell, there are several approaches attempted, for example, light trapping techniques such as texturing the bottom surface, usage of transparent conductor in the superstrate-type cells, and a metal texturing in substrate type cells [1, 2].

Silicon is a semiconductor material which consists of some metal elements and some of those of are electrical insulators, making it suitable to be used in solar cell fabrication [3]. Porous silicon (PS) is a nanostructure formed on a silicon substrate. PS has a capability to be used in many fields including microelectronics, optoelectronics, and photovoltaic. There are several techniques to form the porous silicon such as the electrochemical dissolution of silicon wafer using electrolytic containing hydrofluoric acid (HF) and ethanol, laser assisted etching and electroless etching, electrochemical

etching using DC current, electrochemical etching using AC current, and stain etching [4–8]. The process to construct the porous silicon is economical and suitable for mass production [9]. In producing high efficiency of the solar cell, porous silicon can be used as antireflection coating (ARC) layer.

According to Nakamura et al. [10], there are several output parameters that need to be considered for measuring the performance of solar cell, which is maximum power (P_{\max}), fill-factor (FF), short-circuit current (I_{sc}), and open-circuit voltage (V_{oc}). According to Ramizy et al. [11] the porous silicon has an effective feature that can improve the solar cell performance. Ramizy et al. [9] obtained the porous structure surfaces that contains discrete pores and short-branched pores at the top surfaces while smaller pore size and random pores at the bottom surfaces of the solar cell. These double porous structures showed enhanced conversion efficiency of the solar cell. This motivated the work to simulate the single and double porous structures to investigate its possibilities to enhance the efficiency of silicon solar cell. The performance will be compared with the experimental work of Ramizy et al. [9].

2. Experimental details

In this work, three structures of the silicon solar cell were constructed using Silvaco TCAD software. The three structures are no porous (Si *p*-type solar cell), single porous (*n*-PS/*P* solar cell), and double porous (*n*-PS/*p*-PS solar cell) structures. Athena process sim-

*corresponding author; e-mail: alhan570@uitm.edu.my

ulator was used to construct the no porous and single porous structures while Devedit tool was used to construct the double porous structure. Figure 1 shows the flowchart of this work summarizing the flow in simulating the solar cells. Firstly, an input file was written in Athena and Devedit to construct the three structures. After that, the structures were imported to Atlas device simulator for the characterization of the solar cell performances.

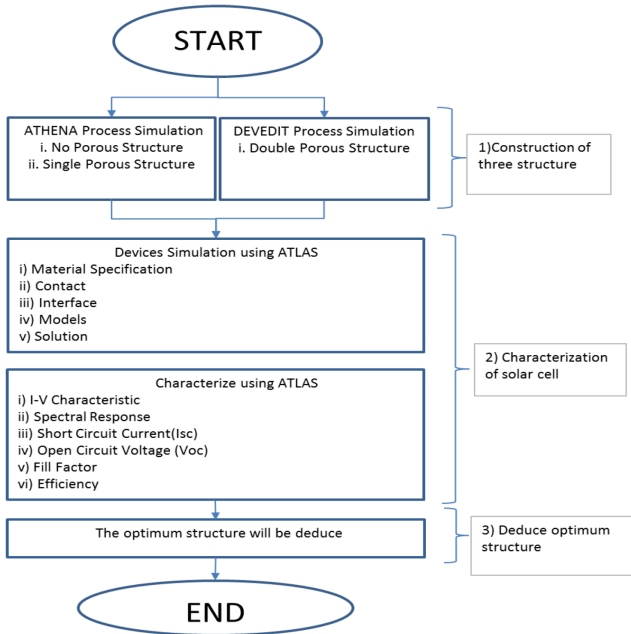


Fig. 1. Flow chart for simulation of solar cell structures and its characterization.

The results in term of current–voltage (I – V) characteristics, spectral response, and power curve were obtained from the simulation. Finally, performance parameters of the solar cells (I_{sc} , V_{oc} , P_{max} , FF, and efficiency) were extracted from the I – V curve and the optimum structure will be deduced from these parameters.

2.1. Athena process simulation for no porous and single porous

Athena is a process simulator which was used in constructing and simulating the no porous and single porous structure. At the beginning of this simulation, an input file was written. In the input file, a p -type silicon wafer (doped with boron of $1.8 \times 10^{16} \text{ cm}^{-3}$ concentration) was initialized and the mesh was defined by setting the x - and y -mesh. The size of the region is $10 \mu\text{m}$ (width) by $100 \mu\text{m}$ (depth). The fine mesh was defined at the active region (from top surface to junction) whereas coarse mesh was tabulated at the bottom of the substrate. This was done so that the device characteristic will be simulated accurately and timely. The setting of the mesh is as following statement:

```
go athena
Line x loc = 0.00 spac = 1
Line x loc = 10 spac = 1
Line y loc = 0.00 spac = 0.2
Line y loc = 1.5 spac = 0.5
Line y loc = 4.5 spac = 0.5
Line y loc = 100 spac = 0.2
```

For the single porous structure an etching process was carried out to form the pore at the top surface of the Si wafer. Figure 2 shows the non-porous and single porous structures along with the mesh defined.

To make n - p junction, both structures were implanted with phosphorus doping of $1.8 \times 10^{16} \text{ cm}^{-3}$. After the implantation process, the wafers were subjected to annealing of 1500°C for 350 min to drive in the n -type doping. Figure 3 shows the structure of non-porous and single porous with contour doping of n -type concentration (phosphorus). The cut line of the structure depicted the doping profile. The estimated junction depth of the p -type region is about $43 \mu\text{m}$.

Finally, aluminum was deposited at the top of n -type region to create cathode contact and at the bottom of p -type region as the anode contact. The final structures with contact electrode were shown in Fig. 4.

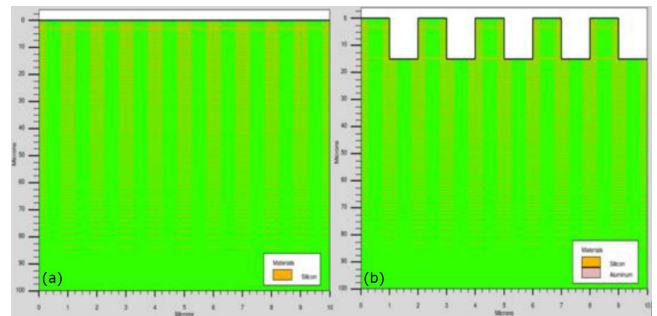


Fig. 2. (a) Non-porous and (b) single porous structures with the mesh definition.

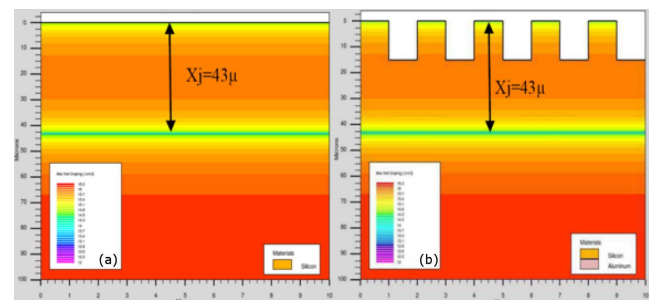


Fig. 3. The structure of (a) non-porous and (b) single porous with contour doping of n -type concentration (phosphorus). The cut line of the structure depicted the doping profile.

TABLE I

ATLAS command groups with the primary statement in each group following the order.

Group	Statements
structure specification	mesh, region, electrode, doping
material model specification	material, models, contact, interface
numerical method selection	method
solution specification	log, solve, load, save
result analysis	extract, tonyplot

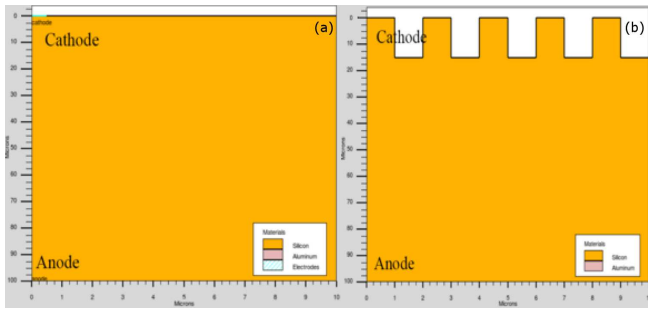


Fig. 4. The structure of (a) non-porous and (b) single porous with contact electrode at the top and bottom.

2.2. Devedit simulation for double porous

Devedit tools were used to create the double porous structure with the porous at the top of n -type region and porous at the bottom of p -type region. Devedit is user friendly tool, whereby user can directly create the structure without the need to optimize the process details. Firstly, the work size area was specified according to the solar cell structure which is $10 \mu\text{m}$ by $100 \mu\text{m}$. Silicon material was used to construct the porous n -type and p -type regions. The doping was set for the n -type and p -type region with the concentration of $1.8 \times 10^{16} \text{ cm}^{-3}$ of phosphorus and boron, respectively. After that aluminum was deposited at the top and bottom of n -type and p -type porous regions for the cathode and anode contacts. Finally, the final drawn structure of double porous solar cell was saved in .str file which will be called in the Atlas device simulator. Figure 5 shows the structure of the double porous solar cell constructed in Devedit.

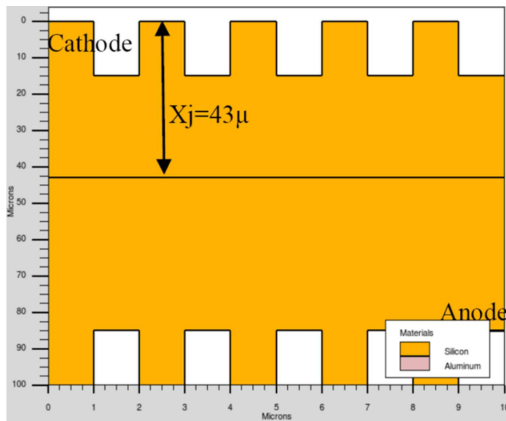


Fig. 5. The structure of double porous silicon solar cell with contact electrode at the top and bottom.

2.3. Devices simulation using ATLAS tools

ATLAS device simulator was used to simulate device performances of the three structures constructed using Athena and Devedit. The statement used in the simulation of the structures in ATLAS were defined following the order stated in Table I.

Mesh infile command was used to load the structure file build in Athena and Devedit. Material command was used to specify the physical properties of the material and the contact. The light source or beam to the solar cell was set at the top and bottom of the structure by setting up the beam power and its wavelength. Finally, the biasing of the device was carried out by setting the numerical method selection and solution specification as shown in the following statements:

```
models conmob fldmob consrh print
solve init
solve previous
```

Figure 6 shows the solar cell structure with respective beam shining at the top and bottom surfaces.

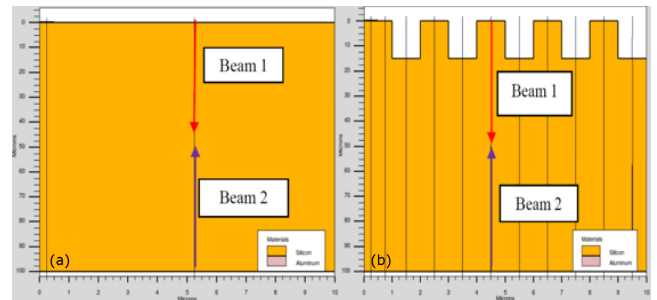


Fig. 6. Illumination of light source to the solar cell structures: (a) non-porous and (b) single porous.

Finally, the performance parameters of the solar cell were extracted from the $I-V$ curve obtained. Tony plot was used to display the simulated structures and the $I-V$ characteristics.

3. Results and discussion

The final structure of non-porous, single porous, and double porous were shown in Fig. 7, respectively. The diameter of the pore is $1 \mu\text{m}$ and the depth of the pore is $15 \mu\text{m}$ for the porous structures. These structures was embedded in the ATLAS simulation for the device characterization.

Spectral response is the ratio of the current generated by the solar cell to the power incident on the solar cell. Figure 8 shows the spectral response for the



Fig. 7. Structures of the three solar cells: (a) non-porous, (b) single porous, and (c) double porous.

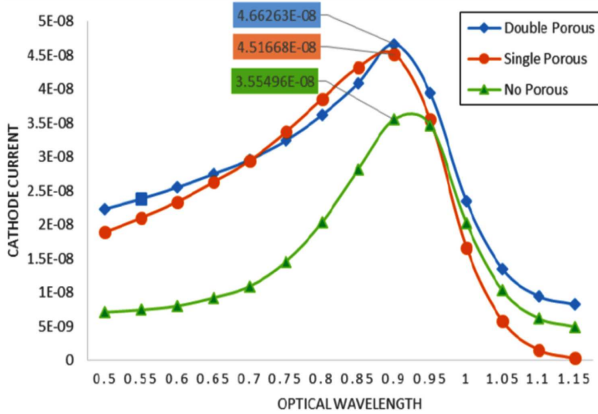


Fig. 8. Spectral response of the non-porous, single porous, and double porous structure.

three structures. Generally, the three solar cells exhibited significance response spanning from $0.5 \mu\text{m}$ to about $1.1 \mu\text{m}$, covering the broad visible light spectrum. Specifically, non-porous structure exhibited peak response at $0.925 \mu\text{m}$, single porous at $0.9 \mu\text{m}$, and double porous at $0.9 \mu\text{m}$, respectively. The double porous solar cell showed the highest response ($I = 4.66 \times 10^{-8} \text{ A}$) towards light at the near infrared region. This indicates that the double porous has the highest absorption and low reflection compared to the other two structures due to the increase of porosity that leads to the increase in the PS density over the surface of the sample which enhances the trapping of the light [9].

Internal quantum efficiency (IQE) is the efficiency with which photons that are not reflected or transmitted out of the cell that generates collectable carriers. Figure 9 shows the IQE graph for three structures. At the wavelength $0.5 \mu\text{m}$, surface recombination process occurred for all the structures and the structures reduce to absorb

the light at $1.1 \mu\text{m}$ wavelength. Comparing the three structures, double porous structure shows the highest peak of the generating collectible carriers of 0.35, single porous of 0.33 at $0.9 \mu\text{m}$ wavelength and the non-porous of 0.32 at $0.95 \mu\text{m}$ wavelength, respectively. According to Ramizy et.al [9], porous silicon form at both porous layers have lower reflectivity compared to the single porous layer.

Figure 10 shows the external quantum efficiency (EQE) for the non-porous, single porous, and double porous structures. EQE is the effect of optical loss such as transmission and reflection. By comparing the peak of the ratio of current and source photocurrent, double porous exhibited the highest peak which is 0.66, single porous of 0.62, and non-porous of only 0.29 at about $0.9 \mu\text{m}$ wavelength. Porous silicon on the both surfaces acting as effective anti-reflective layer (ARC) by reducing the reflection and increasing the conversion productivity [8].

Figure 11 shows the dark $I-V$ and light $I-V$ for the double porous, single porous, and non-porous structures. Dark $I-V$ curve was used in solar cell analysis to rely on superposition principle. The light $I-V$ curve is the dark $I-V$ curve shifted by the light generating current. At the dark $I-V$ curve, there is no generating current.

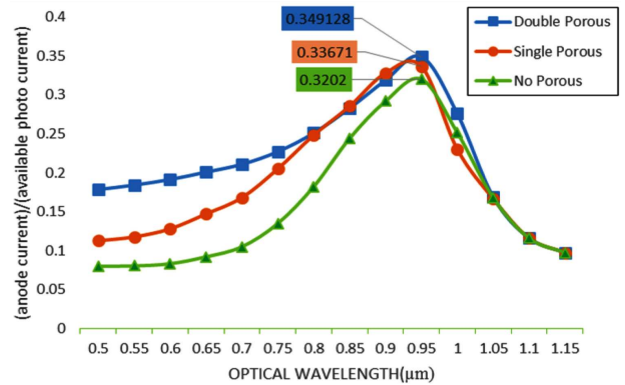


Fig. 9. IQE graph for non-porous, single porous, and double porous structure.

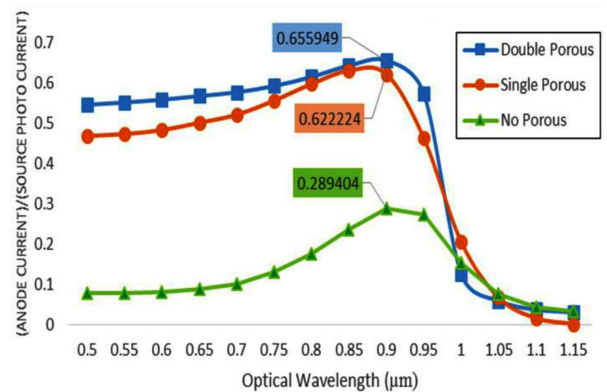


Fig. 10. EQE graph for non-porous, single porous, and double porous structure.

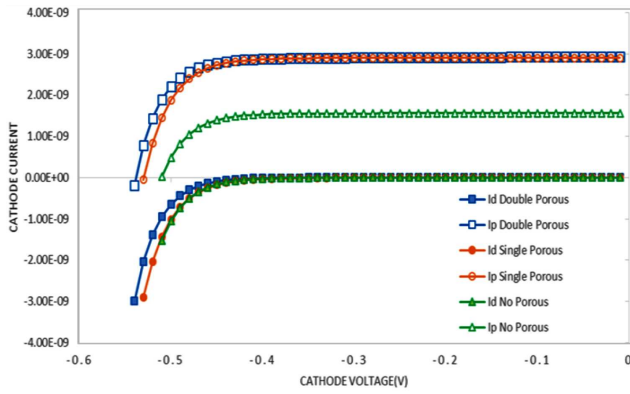


Fig. 11. Dark $I-V$ and light $I-V$ for non-porous, single porous, and double porous structure.

Double porous structure shows the highest generating current of 2.93×10^{-9} A, single porous at 2.90×10^{-9} A, and non-porous 1.56×10^{-9} A.

Figure 12 shows the maximum power curve for the non-porous, single porous, and double porous structure. The peak of the curve shows the maximum power produced by the structures. Double porous structure exhibited higher peak at 1.26 nW, single porous at 1.23 nW, and non-porous at 6.34 nW.

The photovoltaics properties for the three structures of simulated solar cell and fabricated solar cell of Ramizy et al. [9] are summarized in Table II. A remarkable increase could be observed in the short circuit photocurrent and open circuit voltage of the silicon solar cell when there is non-porous structure at 1.56 nA, 0.51 V, single porous at 2.90 nA, 0.53 V, and double porous at 2.93 nA, 0.54 V from the simulation results. The fill factor for the

three structures of simulation results is 0.8. The fill factor is defined as the ratio of the maximum power from the solar cell to the product of open circuit voltage and short circuit photocurrent. The fill factor is measure of the “squareness” of the solar cell and is also the area of the largest rectangle which will fit in the $I-V$ curve. The double porous for the simulation result and fabrication result has the highest efficiency compared to the non-porous and single porous structure which is 9.55%, and which is comparable with the fabricated solar cell of 12.75% efficiency. This slight difference might be due to the mesh definition of simulated structures which different from the actual wafer in fabrication process. The double porous at the surface of solar cell structure can be used as ARC layer in producing the high efficiency of the solar cell.

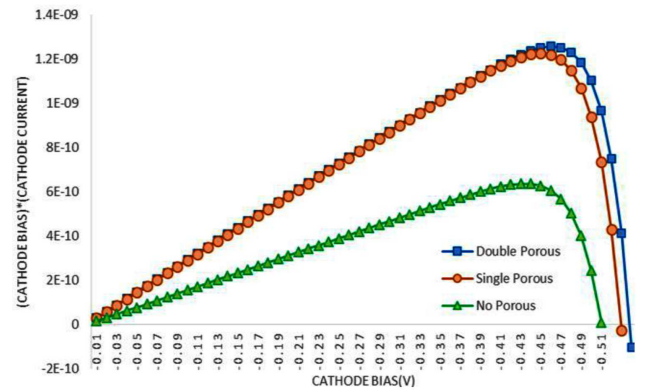


Fig. 12. Power curve for non-porous, single porous, and double porous structure.

TABLE II

The photovoltaic properties for the three structure of simulated solar cell and fabrication solar cell.

	Simulation results			Ramizy et al. [9]		
	No porous	Single porous	Double porous	No porous	Single porous	Double porous
I_{sc} [mA]	1.56	2.90	2.93	6.72	8.83	12.37
V_{oc} [V]	0.51	0.53	0.54	0.31	0.43	0.49
P_{max} [W]	0.64n	1.23n	1.26n	1.73m	2.96	5.33m
fill factor	0.80	0.80	0.80	0.83	0.78	0.88
efficiency	4.84	9.32	9.55	4.34	7.38	12.75

4. Conclusions

The efficiency of silicon solar cell is improved by using the porous structure at the top and bottom surfaces. The simulation result and fabrication result show that the porous silicon at the both sides is more efficient compared to the single porous structure and non-porous structure. This study indicates that the porous silicon is suitable to be used as ARC layer by reducing the light reflection and increase of the light absorption by the solar cell. For the future work, the depth of the porous should be investigated to prevent surface recombination which could

lower the quantum efficiency and the creation of more porous by reducing the diameter of the porous to trap more photons.

Acknowledgments

Support from Universiti Teknologi MARA (UiTM) and IC Design laboratory UiTM Pulau Pinang staffs are gratefully acknowledged. The authors would like to acknowledge the financial support from Ministry of Higher Education Malaysia (MOHE) through Fundamental Research Grant Scheme (600-RMI/FRGS 5/3(0107/2016)).

References

- [1] B.L. Sopori, J. Madjdpour, W. Chen, Y. Zhang, *AIP Conf. Proc.* **462**, 291 (1999).
- [2] H.S. Radhakrishnan, Chihak Ahn, N. Cowern, K. Van Nieuwenhuysen, I. Gordon, R. Mertens, J. Poortmans, in: *Proc. IEEE 39th Photovoltaic Specialists Conf. (PVSC), Tampa (FL)*, 2013, p. 0058.
- [3] M.F. Nayan, S.M.S. Ullah, S.N. Saif, in: *Proc. 3rd Int. Conf. on Electrical Engineering and Information Communication Technology (ICEEICT), Dhaka*, 2016, p. 1.
- [4] S. Yaakob, M.A. Bakar, J. Ismail, N.H. Hanif Abu Bakar, K. Ibrahim, *J. Phys. Sci.* **23**, 17 (2012).
- [5] A. Ramizy, Z. Hassan, K. Omar, *Mater. Lett.* **65**, 61 (2011).
- [6] N.H.A. Wahab, A.F.A. Rahim, A. Mahmood, Y. Yusof, *AIP Conf. Proc. ICAPE2016* **1875**, 020002 (2017).
- [7] R. Radzali, M.Z. Zakariah, A. Mahmood, A.F.A. Rahim, Z. Hassan, Y. Yusof, *AIP Proc. ICAPE2016* **1875**, 020003 (2017).
- [8] J. Xu, A.J. Steckl, *IEEE Electron Dev. Lett.* **15**, 507 (1994).
- [9] A. Ramizy, Z. Hassan, K. Omar, Y. Al-Douri, M.A. Mahdi, *Appl. Surf. Sci.* **257**, 6112 (2011).
- [10] T. Nakamura, M. Imaizumi, S.I. Sato, T. Ohshima, in: *Proc. 38th IEEE Photovoltaic Specialists Conf., Austin (TX)*, 2012, p. 002846.
- [11] A. Ramizy, Z. Hassan, K. Omar, *J. Mater. Sci. Mater. Electron.* **22**, 717 (2011).